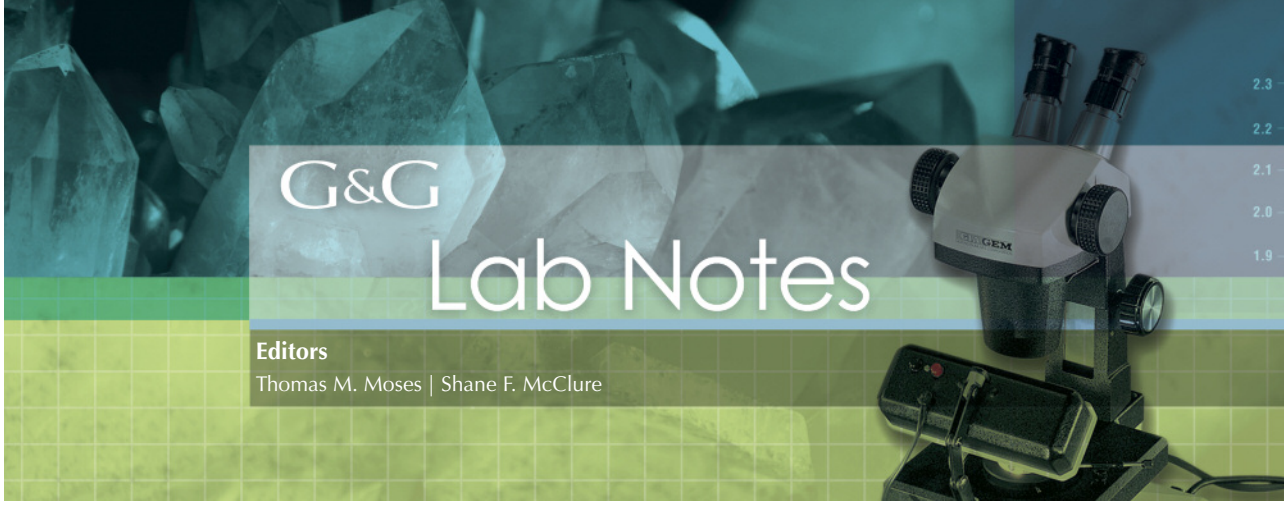

DIAMOND

Artificially Irradiated and Coated Brown

Red is arguably the rarest and most valued color in diamond. It is known to bring record-breaking prices at auction, as in the case of the 0.95 ct Hancock Red, which sold for nearly $1 million per carat in 1987. Some will go to great lengths to achieve this color, even resorting to unusual multiple treatments.

The New York laboratory recently examined a Fancy reddish brown 0.28 ct round brilliant diamond submitted for color origin identification (figure 1). Spectroscopic analysis immediately revealed that it had been artificially irradiated to create the reddish brown color. The presence of an amber center, identified by infrared spectra, indicated that this diamond was likely brown prior to treatment. Further investigation using the DiamondView determined that the stone's pavilion facets had also been coated, a feature not apparent with microscopic observation. DiamondView images displayed weak luminescence, with more intense luminescence concentrated at facet edges, junctions, and where the stone had been scratched. Boiling removed the coating, eradicating the red component and changing the color grade to Fancy Dark orangy brown.

Figure 1. The diamond with a Fancy reddish brown color (left) was revealed to be Fancy Dark orangy brown once the coating and red hue were removed (right).

Removing the coating also produced a much more luminescent DiamondView image (figure 2).

This stone indicates an attempt to induce red color in diamond, presumably to increase the value. Although

Figure 2. DiamondView images of the diamond with the coating (top row) and after the coating's removal (bottom row). The dark spots in the bottom left image are remnants of the coating substance.

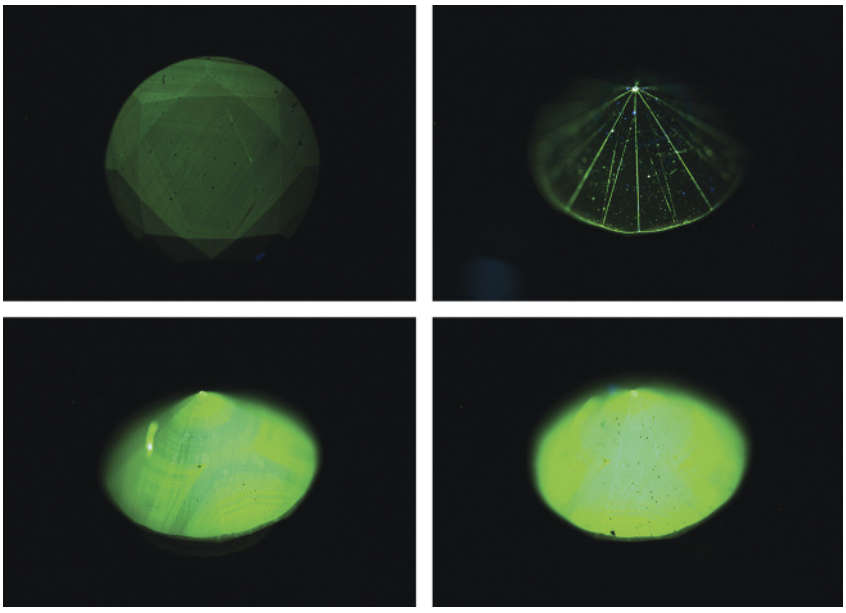

Editors' note: All items were written by staff members of GIA laboratories.

Gems & Gemology, Vol. 50, No. 3, pp. 236–243.

© 2014 Gemological Institute of America

this effort proved unsuccessful, it emphasizes the need for vigilance when analyzing diamonds with rare color. Their appeal, and the number of treatment techniques to create these colors, is sure to grow.

Martha Altobelli, Paul Johnson, and Jason Darley

Mixed-Type Cape Diamond

Natural yellow type Ia or "cape" diamonds, the most common of all colored diamonds, are identified by the N3 (415 nm) and N2 (478 nm) absorption lines in the UV-visible range. These defects produce the characteristic yellow hue, and the N3 line produces the blue luminescence, so often observed in these stones. Weaker bands at 452 and 465 nm may also be visible (C.M. Breeding and J.E. Shigley, "The 'type' classification system of diamonds and its importance in gemology," Summer 2009 *G&G*, pp. 96–111).

The New York laboratory recently examined a 2.16 ct Fancy orangy yellow diamond (figure 3) with unusual features for a cape stone. When analyzed with a UV-Vis spectrometer, it exhibited a cape spectrum and an unexpected 480 nm band, a defect usually associated with orange color (figure 4). Infrared spectrometry revealed a well-defined IaA>B diamond, as opposed to the saturated Ia spectrum typically associated with cape diamonds. These abnormal features prompted further testing, and the DiamondView revealed zoned blue and yellow fluorescence (figure 5). Raman spectroscopy of the transparent, elongated crystal within the diamond, visible in the DiamondView, identified it as a colorless garnet, a common inclusion in cape diamonds.

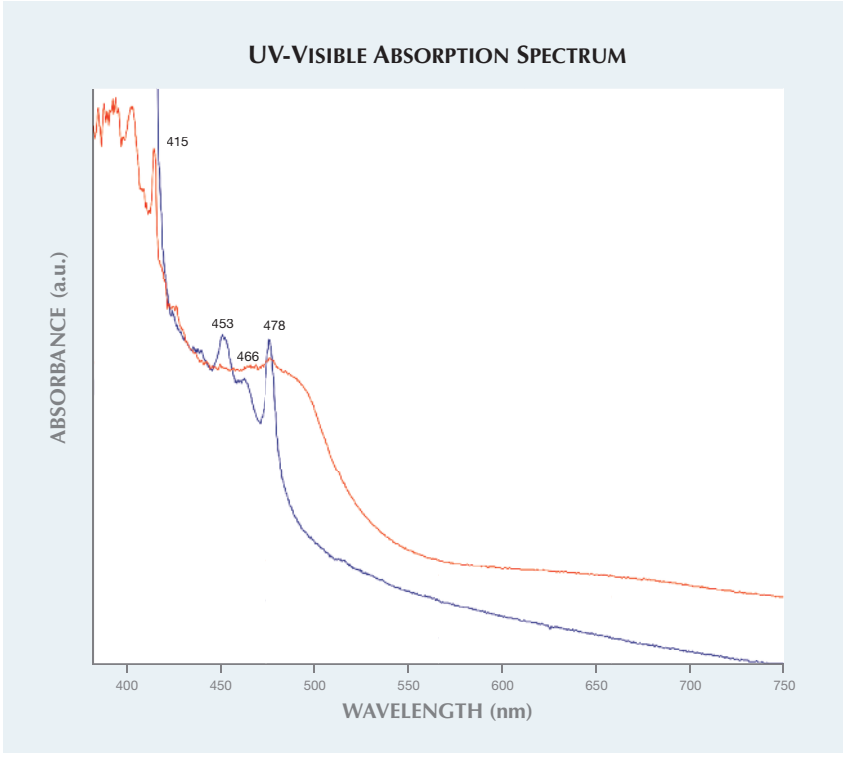

Figure 4. The Fancy orangy yellow diamond's "mixed" cape spectrum (red) is shown along with an overlay of a normal cape spectrum (blue).

Figure 3. This 2.16 ct Fancy orangy yellow diamond is a mixed-type IaA>B.

Figure 5. The cape diamond's DiamondView image displays blue and yellow fluorescence, along with an elongated crystal.

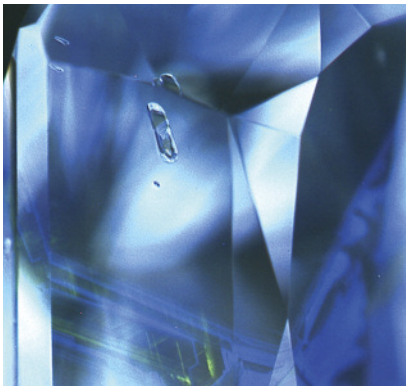

While the specific structure of the 480 nm optical defect is not yet understood, it is known to be associated with yellow fluorescence (Y. Luo and C.M. Breeding, "Fluorescence produced by optical defects in diamond: Measurement, characterization, and challenges," Summer 2013 *G&G*, pp. 82–97). The defect is also sometimes attributed to substitutional oxygen in type I diamonds. From our data and test results showing no evidence of laboratory-produced alteration, we can conclude that this stone is a natural and very rare example of a cape diamond mixed with a 480 nm band causing the orange component.

Martha Altobelli and Paul Johnson

Xenotime Inclusion in Yellow Diamond

Diamond inclusions can be analyzed using Raman spectroscopy, ideally when they are close to or breaking the surface. The New York lab recently

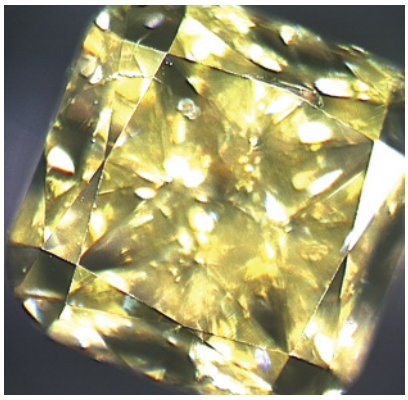

Figure 6. This 0.55 ct yellow diamond contained a rare mineral inclusion of xenotime.

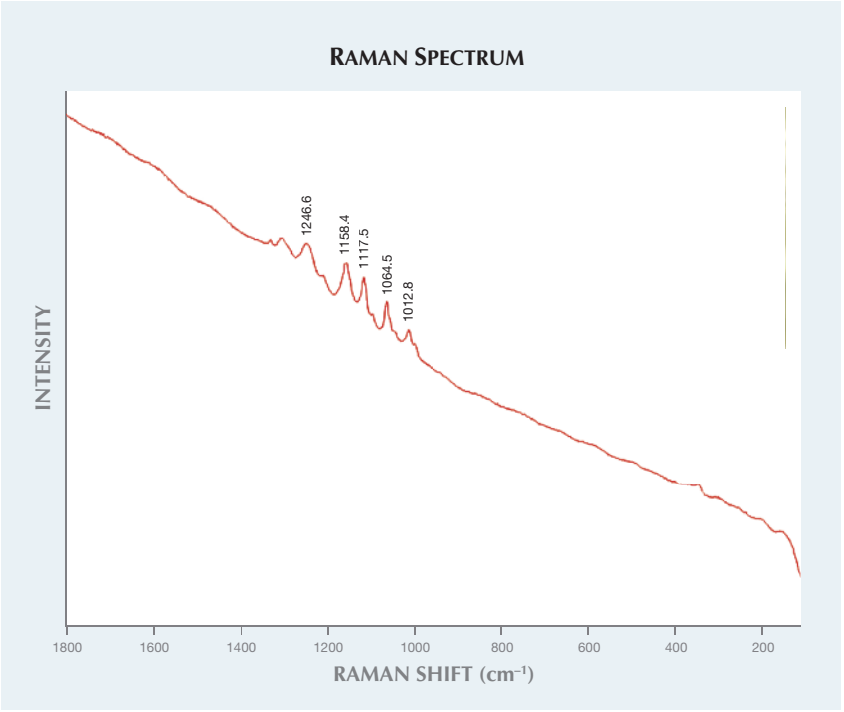

Figure 7. The xenotime inclusion broke through the pavilion surface (inset; magnified 80×). Radiation stains were also observed at the contact with the host diamond (see arrow). The Raman spectrum, using a 514 nm laser, shows xenotime peaks at 1012.8, 1064.5, 1117.5, 1158.4, and 1246.6 cm^{-1}.

had the opportunity to study a rare inclusion of xenotime protruding from the surface of a 0.55 ct Fancy Intense yellow diamond (figure 6).

The yellowish brown inclusion was located in the pavilion near the girdle; radiation stains were observed at the contact area with the host diamond (figure 7, inset). Radiation stains and the nature of the surface penetration suggested that it formed inside an etch channel as an epigenetic inclusion. Raman spectroscopy showed peaks consistent with xenotime at 1012.8, 1064.5, 1117.5, 1158.4, and 1246.6 cm^{-1} as seen in the figure 7 spectrum.

Minerals that formed outside of the diamond stability field can be found inside a diamond (see Spring 2009 Lab Notes, pp. 54–55). Xenotime (yttrium orthophosphate, YPO_4) occurs mainly in granitic pegmatite and also in metamorphic rocks such as biotite gneiss (E.J. Young and P.K. Sims, *Petrography and Origin of Xenotime and Monazite Concentrations, Central City District, Colorado*, Geological Survey Bulletin 1032-F, 1961, pp. 273–297). Young and Sims proposed that granitic fluids such as granodiorite mobilized rare earth elements (REE) and phosphates from biotite gneiss in Colorado. Later, these ions crystallized to form unusually high concentrations of xenotime and monazite in migmatized parts of gneiss. The granitic fluids may have percolated within diamond deposits in continental crust, and REE ions could have been deposited and crystallized inside etch channels, as observed in this yellow diamond. Radiation stains associated with xenotime, which is one of the few naturally occurring yttrium minerals, may contain trace amounts of uranium and be slightly radioactive.

Associations of xenotime with diamond have been previously reported. E. Hussak described intergrowths of monazite and xenotime in diamond-bearing sands in Brazil ("Mineralogische Notizen aus Brasilien," *Tschermaks Mineralogische und Petrographische Mitteilungen*, Vol. 18, 1899, p. 346). More recently, xenotime inclusions have been reported in carbonado from the Macaubas River in Minas Gerais (M. De Souza Martins, *Geologia dos Diamantes e Carbonados Aluvionares da Bacia do Rio Macaubas (MG)*, Ph.D. thesis, Universidade Federal de Minas Gerais, Instituto de Geociencias, Belo Horizonte, Brazil, 2006). To the best of our knowledge, xenotime inclusions in gem-quality diamond have never been reported.

Kyaw Soe Moe, Martha Altobelli, and Paul Johnson

CVD SYNTHETIC DIAMOND with Unusual Inclusions

A 0.34 ct square modified brilliant was submitted to GIA's Carlsbad lab as a synthetic diamond. The specimen, which exhibited good polish and symmetry, received a color grade of K and a clarity grade of SI_2. During advanced testing, the photoluminescence spectra displayed a large 737 nm doublet, a silicon vacancy peak seen in CVD synthetic diamonds. A DiamondView image showed subtle growth dislocations on the pavilion and almost no growth layer structure on the crown (figure 8). A mid-IR spectrum did not show the 3123 cm^{-1} peak, once considered characteristic of CVD synthetics (P.M. Martineau et al., "Identification of synthetic diamond grown using chemical vapor

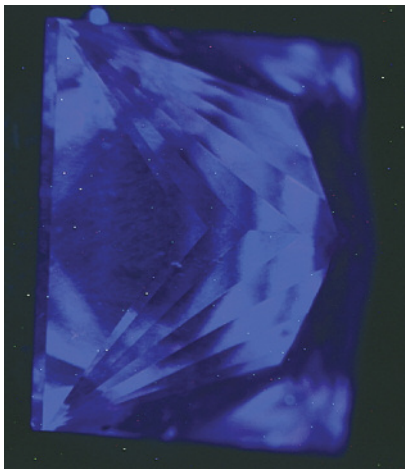

Figure 8. This DiamondView image of the 0.34 ct CVD synthetic shows a pattern of growth dislocations.

deposition [CVD]," Spring 2004 *G&G*, pp. 2–25).

The most unusual features were the inclusions. As seen in figure 9, this item is deserving of its SI_2 clarity grade. In addition to several fractures, there were numerous indented crystal surfaces and included growth remnants. A close-up of the indented crystal surfaces revealed an irregular shape and surface texture (figure 10). The fully included growth remnants lacked any discernible pattern or regularity. Inclusions have been reported in CVD synthetic diamonds, but they have been confined to growth planes (Spring 2013 Lab Notes, pp. 47–49). This specimen's inclusions, which were scattered in a random way,

Figure 9. The pavilion displayed a wide variety of inclusions. Field of view 3.6 mm.

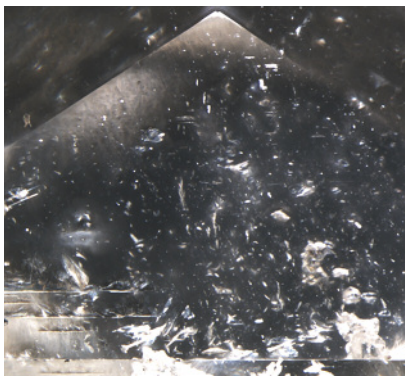

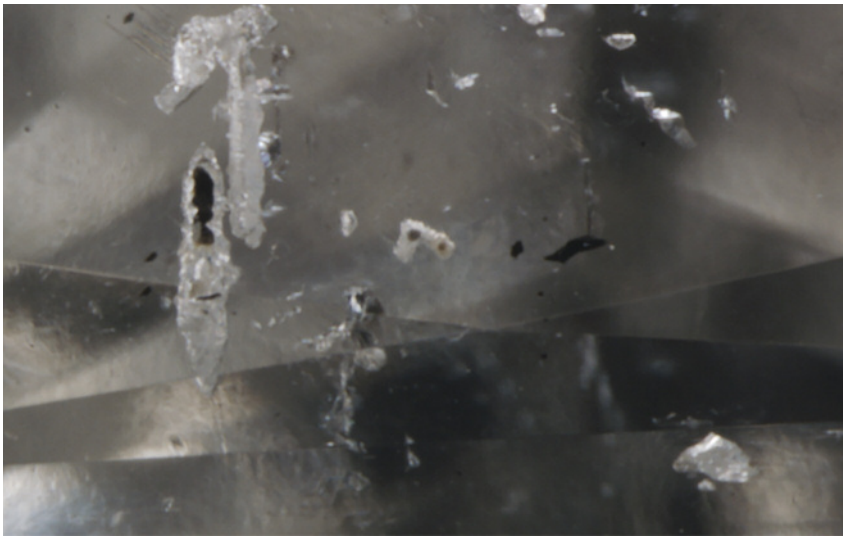

Figure 10. A close-up of some of the indented crystal structures showed etch-like patterns. Field of view approximately 1.4 mm.

showed no uniformity in size, shape, color, or placement. They were whitish or black, pinpoint-sized and larger structures (as seen in figure 10, lower right). Some were flat and pointed, while others were more rounded in shape. Furthermore, some were grouped together, similar to cloud-like inclusions, while others were freestanding, mimicking the inclusion distribution in natural diamond. The strain was mottled around the inclusions and crosshatched in cleaner areas.

The chemical structure and composition of these inclusions is unknown, and why they formed this way is a mystery. It is possible that this material is from a new growth method that yields heavily included product. Synthetic diamond research is a rapidly growing field; as it expands, many new and different types of samples find their way into the trade. The inclusions in this specimen could pass for natural inclusions if observed with a standard 10× loupe or a quick glance in the microscope. The DiamondView image is also difficult to interpret if one is not accustomed to the many fluorescent patterns CVD synthetic diamonds can display. This case is an important reminder to exercise caution when determining natural or synthetic origin, because some synthetic diamonds in the market look very natural.

Troy Ardon

Two Fancy Dark Gray CVD Synthetic Diamonds

Recently, two colored synthetic diamonds examined in the Carlsbad laboratory were determined to have been grown by the chemical vapor deposition (CVD) method. Both received an unusual color grade of Fancy Dark gray. GIA has graded other gray CVD synthetics before, but within the Fancy Light to Fancy range; it is rare for a synthetic to receive a Fancy Dark color grade. The few Fancy Dark synthetic diamonds submitted in the past have all been HPHT synthetics (most of them Fancy Dark reddish brown) with post-growth treatment that created NV centers. The two gray CVD specimens were also noted for their size—0.80 and 1.50 ct. The latter is shown in figure 11.

In addition to their color grade, both showed similar spectra. Neither sample's UV-visible-NIR spectrum displayed any distinct absorption peaks. The mid-IR spectra identified them as type IIa diamond but did not contain

Figure 11. This 1.50 ct Fancy Dark gray CVD synthetic diamond was unusual for its combination of color grade and large size.

features that confirmed synthetic origin. Their photoluminescence (PL) spectra had nearly identical features, suggesting that they originated from similar manufacturing processes. Both PL spectra featured a large silicon-vacancy doublet at 737 nm, a strong indicator of CVD growth (though natural diamonds will occasionally show a weak silicon peak along with other natural features); this was confirmed by the DiamondView images. The 1.50 ct specimen showed light blue fluorescence and striations commonly observed in CVD synthetics (figure 12, left) (P. Martineau et al., "Identification of synthetic diamond grown using chemical vapor deposition (CVD)," Spring 2004 *G&G*, pp. 1–25). The 0.80 ct sample offered a more unusual DiamondView image, with yellow fluorescence interspersed with regions of purple mottling. The purple mottling is seen occasionally in CVD synthetics, but usually combined with a background of pink fluorescence (W. Wang et al., "Latest-generation CVD-grown synthetic diamonds from Apollo Diamond Inc.," Winter 2007 *G&G*, pp. 294–312) instead of the yellow fluorescence seen here. Some regions of the 0.80 ct synthetic had natural-looking fluorescence features (figure 12, right), but a thorough examination of the DiamondView fluorescence in conjunction with the silicon peak unambiguously identified it as CVD.

The DiamondView images of both synthetics also demonstrated blue phosphorescence, which is often associated with boron impurities. No known boron-related peaks were detected in the PL or mid-IR spectra, so the boron concentration would be below the level of detection by FTIR spectroscopy. Boron-related peaks seen in natural and treated type IIb diamonds often are not detected in known IIb HPHT- and CVD-grown synthetics. It is unclear whether the low boron concentration was deliberately introduced to improve growth rate and quality (S. Eaton et al., "Diamond growth in the presence of boron and sulfur," *Diamond and Related Materials*, Vol. 12, 2003, pp. 1627–1632). Boron-containing diamonds with low color saturation often appear gray, making this element the likely cause of color in both of these CVD synthetic diamonds.

Figure 12. Left: In the DiamondView, the 1.50 ct sample showed the familiar color and striations of CVD synthetics. Right: The 0.80 ct specimen displayed a combination of natural-appearing features in some regions (as shown) and CVD-related striations and purple mottling in others.

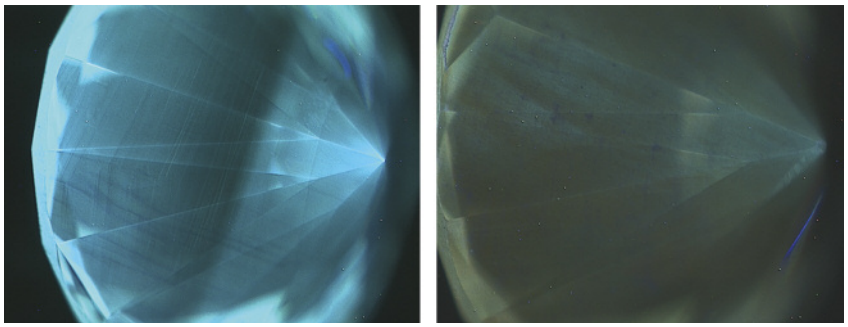

Troy Ardon and
Sally Eaton-Magaña

Heavily Irradiated CVD Synthetic Diamond

A Fancy Deep gray-blue diamond weighing 0.46 ct was submitted to the Carlsbad lab for an identification and origin report. Its UV-Vis-NIR spectrum showed a large GR1 center, indicating artificial irradiation. Furthermore, a small 737 nm silicon doublet was seen and later confirmed with photoluminescence (PL) spectroscopy (figure 13). The silicon doublet is a feature in CVD synthetic diamonds, and only very rarely in natural diamonds.

To confirm the synthetic origin of the material, DiamondView images were collected. This required setting the DiamondView at the highest exposure time, because heavily irradiated diamonds tend to show very weak fluorescence, making the image difficult to resolve. The DiamondView image showed a pattern of growth dislocations, which is characteristic of CVD synthetics (figure 14). The infrared spectrum showed some unknown features in the nitrogen region at 1250 and 1116 cm^{-1}. The infrared spectrum lacked the 3123 cm^{-1} hydrogen-related defect diagnostic of CVD growth (P.M. Martineau et al., "Identification of synthetic diamond grown using chemical vapor deposition [CVD]," Spring 2004 *G&G*, pp. 2–25), or the 3107 cm^{-1} peak sometimes created in synthetic diamonds containing hydrogen by HPHT treatment (I. Kiflawi et al., "The creation of the 3107 cm^{-1} hydrogen absorption peak in synthetic diamond single crystals," *Diamond and Related Materials*, Vol. 5, 1996, pp. 1516–1518).

CVD synthetic diamonds are known to be treated post-growth to improve color, but this has been seen as HPHT treatment or a combination of irradiation and annealing. HPHT treatment of a CVD synthetic diamond can partially or completely re-

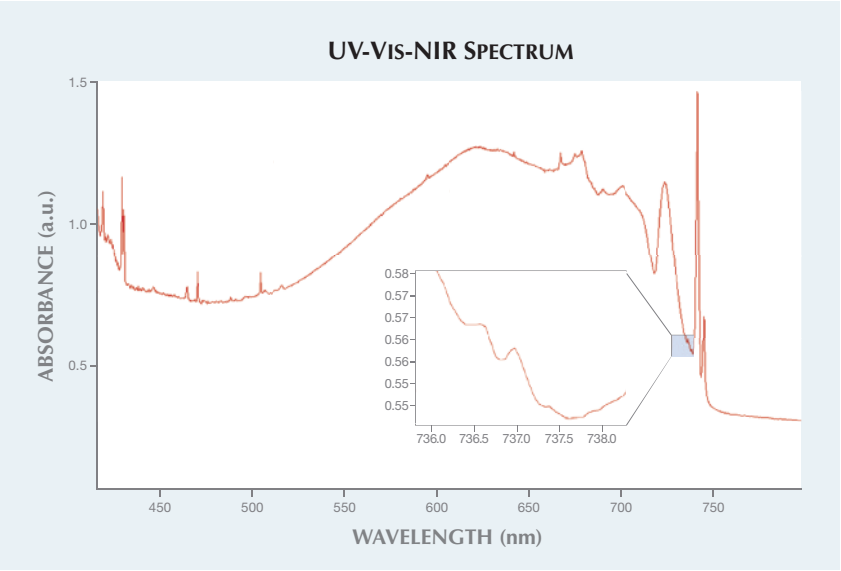

Figure 13. The visible-NIR spectrum of the 0.46 ct irradiated synthetic diamond showed a clear Si-doublet at 737 nm.

move a brownish color created during the growth process. If a CVD synthetic is grown with nitrogen impurities, irradiation and annealing will create nitrogen-vacancy centers, producing a pink to red color (J. Shigley et al., "Lab-grown colored diamonds from Chatham Created Gems," Summer 2004 *G&G*, pp. 128–145).

This is the first CVD synthetic examined at GIA that has been irradiated to a blue color. The fact that the diamond is synthetic automatically means that the irradiation was done in a laboratory; however, the material displayed color zoning near the culet in a manner identical to natural diamonds that have been irradiated artificially. Electron paramagnetic resonance determined a 20 (+/- 5) ppb concentration of isolated nitrogen. If the specimen were to be annealed, the vacancies would combine with the nitrogen to form NV^- centers, as mentioned above. It is possible that the diamond was submitted in an intermediate phase before the final treatment, or that the owner believed it to be a natural but treated stone. Indeed, in the absence of PL spectroscopy and DiamondView images, this specimen could easily be mistaken for an irradiated natural diamond.

As CVD synthetics become more prevalent and subject to a wider variety of treatments, it will only reinforce the role of the gemological laboratory as the most reliable way to separate synthetic from natural diamonds.

Troy Ardon and Wuyi Wang

Figure 14. With DiamondView imaging, the growth dislocations in the irradiated CVD synthetic diamond can be clearly seen as the blue sections among the green fluorescence.

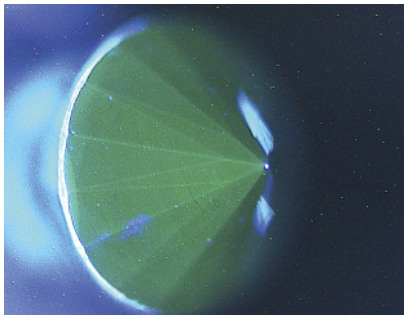

Natural PEARLS Reportedly from a *Spondylus* Species ("Thorny" Oyster)

Non-nacreous conch, clam, *Melo melo*, *Cassis*, and scallop pearls are often submitted to GIA for identification. Four non-nacreous pearls, weighing 5.72 to 12.40 ct and measuring from 9.55 × 8.60 mm to 16.35 × 9.36 mm, were recently submitted to GIA's New York laboratory for identification. These examples caught our attention because of their unusual appearance (figure 15).

Their bodycolors and shapes varied. Each exhibited some degree of pink and orange hues, and either elongated or button shapes. The porcelaneous surfaces also exhibited areas with clear flame structures. Under fiber-optic light, fine flame structures resembling those seen in other porcelaneous pearls such as *Tridacna gigas* and *Strombus gigas* (conch) pearls were observed. While the typical whitish flame structure was readily

Figure 15. Four non-nacreous pearls, weighing 12.40, 11.55, 8.22, and 5.72 ct (left to right), were submitted for identification.

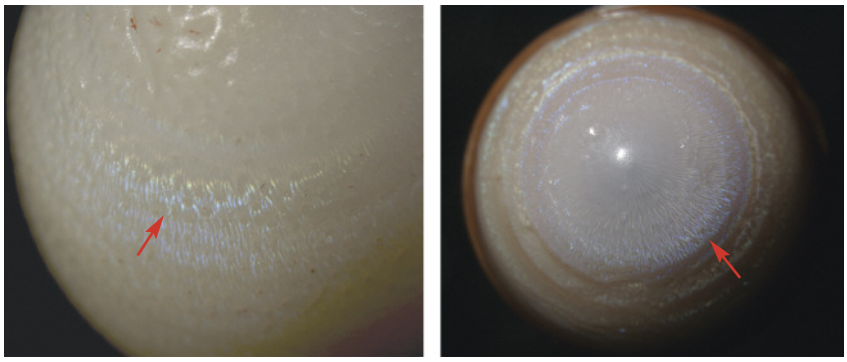

Figure 16. The porcelaneous surface appearances of two of the pearls, weighing 12.40 ct (left, magnified 20×) and 8.22 ct (right, magnified 10×) show their characteristic blue flames, indicated by the arrows.

apparent, the more notable observation was that some of the flames had a distinct blue coloration (figure 16). Other types of pearls usually do not show blue flames. Microradiography was of little diagnostic assistance, as only tight structures were observed; this is not unusual for porcelaneous pearls. Raman spectroscopy detected both aragonite and calcite separately on different parts of the samples. In the authors' experience, this differs from conch or clam pearls, which are usually composed of aragonite only.

Due to their unique shapes, colors, surface, and flame structures, we suspected these pearls were from one of the many *Spondylus* species (figure 17), commonly called "thorny" or "spiny" oysters. Although rarely encountered in GIA laboratories, *Spondylus* pearls have been documented in the past (Winter 1987 Lab Notes, p. 235; E. Strack, *Pearls*, Ruhle-Diebener-Verlag GmbH & Co., Stuttgart, 2006, p. 255), and some samples have been collected by the Qatar Museums Authority (H. Bari and D. Lam, *Pearls*, Skira Editore S.p.A, 2009, pp. 88–89). Our client later informed us that these specimens were found by a fisherman in shells of *Spondylus princeps* off the coast of Baja California, Mexico.

This was a rare opportunity to see natural pearls from a known *Spondylus* species, and to document their unique gemological characteristics as references for mollusk identification in the future.

Figure 17. These shells are from various Spondylus *species. Courtesy of GIA's Bangkok laboratory.*

Joyce WingYan Ho and Chunhui Zhou

Flame-Fusion SYNTHETIC RUBY Boule with Flux Synthetic Ruby Overgrowth

Synthetic rubies with both curved growth and flux-type inclusions in a single stone occasionally appear in the trade. Often these are flame-fusion synthetics that have been quench-crackled and flux-healed to produce a more "natural" appearance. In other instances, flame-fusion material may be used as a seed for flux corundum overgrowth. If the seed crystal is not removed during cutting, it becomes part of the faceted synthetic gemstone (R.E. Kane, "A preliminary report on the new Lechleitner synthetic ruby and synthetic blue sapphire," Spring 1985 *G&G*, pp. 35–39).

The Carlsbad laboratory recently examined a 249.78 ct transparent to semi-transparent rough red crystal (figure 18). Standard gemological testing using a handheld spectroscope revealed a typical ruby spectrum. Observed with a dichroscope, the rough crystal displayed medium orange red to purplish red pleochroism and fluoresced strong red to long-wave UV and medium red to short-wave UV. All of these properties were consistent with ruby.

Microscopic examination using brightfield illumination revealed both curved striae and flux fingerprint patterns (figure 19). Careful examination of one end of the rough crystal showed a noticeable boundary between a flame-fusion core and a flux-grown overgrowth. Part of the core had not been covered by the flux overgrowth (again, see figure 18). The flux fingerprint inclusion penetrated just a few millimeters into the crystal and was only visible in the flux overgrowth (again, see figure 19). What appears to be a pronounced dark grayish reaction zone at the interface of flame-fusion and flux growth was observed (figure 20). The reaction zone

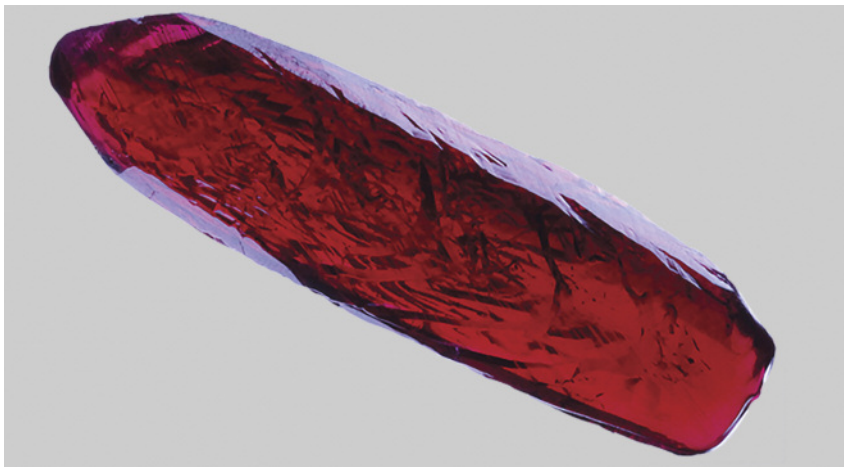

Figure 18. This 73.69-mm-long synthetic ruby crystal is composed of a flame-fusion synthetic ruby boule core with a flux synthetic ruby overgrowth.

likely indicates slight structural and chemical variations between the flame-fusion core and the flux overgrowth. When a new crystal is grown on top of an old crystal, the new growth starts on an irregular surface that was created when the old surface was melted back slightly at the melt temperature. When growth starts on an irregular surface, it creates a nonperfect crystal lattice match between the original seed and new overgrowth. This growth boundary face will disrupt the regularity of the structure of the growth crystal and contribute to the presence of the reaction zone (Schmetzer et al., "Flux-grown synthetic alexandrites from Creative Crystals Inc.," 2012, *Journal of Gemmology*, Vol. 33, No. 1–4, pp. 49–81). In areas where the structural and chemical difference was not very distinct, the reaction zone was partially visible as dark grayish color patches (figure 21). The reaction zone looked grayish because the red bodycolor of the ruby masked what is probably a blue color zone caused by Ti-Fe pairs, a well-known defect that causes blue color in corundum (Summer 1991 Lab Notes, p. 112). The blue zone is along the interface of the flame-fusion core and flux overgrowth.

Advanced testing on the rough crystal using energy-dispersive X-ray fluorescence (EDXRF) analysis revealed traces of Ca, Ti, and Cr in the areas both with and without flux overgrowth; Mo was only detected in areas with the flux overgrowth. The concentration of Fe was below the detection limit of EDXRF. This result is consistent with the chemical element differences between flame-fusion and flux synthetics (S. Muhlmeister et al., "Separating natural and synthetic rubies on the basis of trace-element chemistry," Summer 1998 *G&G*, pp. 80–101).

This synthetic ruby specimen is unusual in that regions originating from the two growth methods occur in the same crystal, with the half of the split boule seed crystal composing the bulk of the entire specimen. While flux overgrowth on flame-fusion seed crystals has been previously reported (E.J. Gübelin and J.I. Koivula, *Photoatlas of Inclusions in Gemstones, Volume 2*, Opinion Verlag, Basel, Switzerland, 2005, p. 352), this type of material is rarely seen in GIA's laboratory, and this example was particularly unusual due to its large size.

Ziyin Sun and Heidi Breitzmann

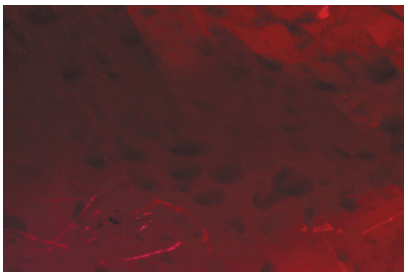

Figure 21. Also observed was a partial reaction zone between the flame-fusion core and the flux overgrowth. Image width 5.85 mm.

Figure 19. Subtle curved striae (right arrow) and fingerprint-like flux residue (left arrow) are indicative of both flame-fusion and flux growth. Image width 6.94 mm.

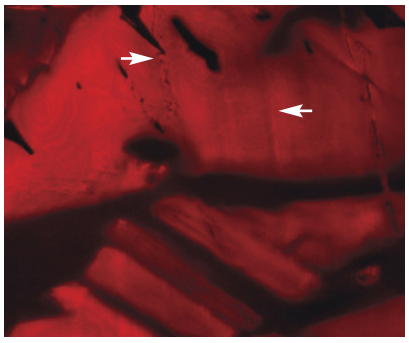

Figure 20. A dark grayish reaction zone was observed between the flame-fusion core and the flux overgrowth. Image width 15.67 mm.

PHOTO CREDITS:
Jian Xin (Jae) Liao—1, 3, and 11; Paul Johnson—2 and 5; Kyaw Soe Moe—6 and 7; Troy Ardon—8, 9 and 10; Sally Magaña—12; Wuyi Wang—14; Sood Oil (Judy) Chia—15; Joyce WingYan Ho—16; Nuttapol Kitdee —17; Nathan Renfro—18, 19, 20, and 21.

G&G

Gem News International

Contributing Editors
Emmanuel Fritsch, *CNRS, Team 6502, Institut des Matériaux Jean Rouxel (IMN), University of Nantes, France* (fritsch@cnrs imn.fr)
Kenneth Scarratt, *GIA, Bangkok* (ken.scarratt@gia.edu)

COLORED STONES AND ORGANIC MATERIALS

Aquamarine with unusually strong dichroism. Recently, a transparent grayish blue oval mixed cut (figure 1) was submitted for identification at the Gem Testing Laboratory in Jaipur. The 4.49 ct stone (12.04 × 8.88 × 7.53 mm) was relatively clean to the unaided eye. Its RI of 1.582–1.590, birefringence of 0.008 with a uniaxial negative optic sign, and hydrostatic SG of 2.71 suggested a beryl, which we later confirmed with FTIR and Raman spectroscopy. The specimen's natural origin was established by planes of dendritic platelets (usually ilmenite) oriented along the basal plane and liquid fingerprints.

The stone's most striking feature was its unusually strong dichroism, displaying deep blue and pale bluish green colors (figure 2). The deep saturated blue resembled that of a top-quality sapphire. Such strong dichroism was reminiscent of Maxixe-type (irradiated) beryls, although their dichroic colors are usually deep blue and colorless. The deep saturated blue was seen along the e-ray, the pale bluish green along the o-ray. Such a pattern of color absorption is associated with aquamarine; the opposite effect occurs in Maxixe-type beryl, which appears colorless along the e-ray and deep blue along the o-ray (R. Webster, *Gems*, 5th ed., Butterworth-Heinemann, London, 1994, pp. 124–127).

Further analysis was performed with UV-Vis-NIR spectroscopy to confirm the cause of color and differentiate between aquamarine and Maxixe-type beryl. Polarized spectra (figure 3) revealed an absorption peak at approximately 427 nm along the o- and e-rays, a typical feature in aquamarine due to the presence of ferric iron (see I. Adamo et al., "Aquamarine, Maxixe-type beryl, and hydrothermal synthetic blue beryl: Analysis and identification," Fall 2008 *G&G*,

Figure 1. This 4.49 ct grayish blue aquamarine was unusual for its strikingly intense dichroism. Photo by Gagan Choudhary.

Figure 2. The dichroic aquamarine displayed unusually intense dichroism, with a deep saturated blue along the e-ray (left) and a pale bluish green along the o-ray (right). The images were taken by fixing the polarizing filter on the camera lens and rotating the polarizer 90 degrees to separate out the two directions. Photos by Gagan Choudhary.

Editors' note: Interested contributors should send information and illustrations to Justin Hunter at justin.hunter@gia.edu or GIA, The Robert Mouawad Campus, 5345 Armada Drive, Carlsbad, CA 92008.

Gems & Gemology, Vol. 50, No. 3, pp. 244–249.

© 2014 Gemological Institute of America

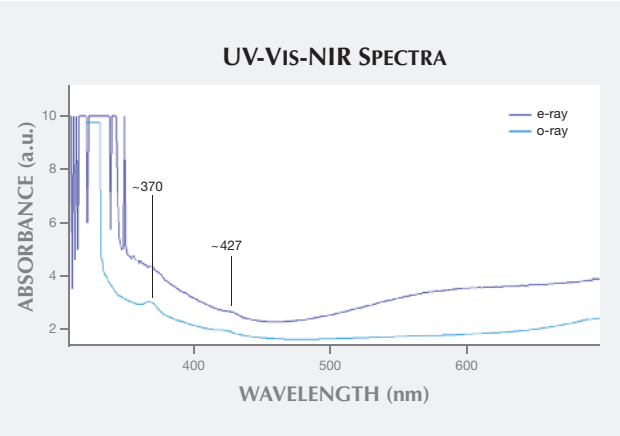

Figure 3. The aquamarine's polarized UV-Vis-NIR spectra displayed Fe^{3+}-related bands at approximately 370 and 427 nm.

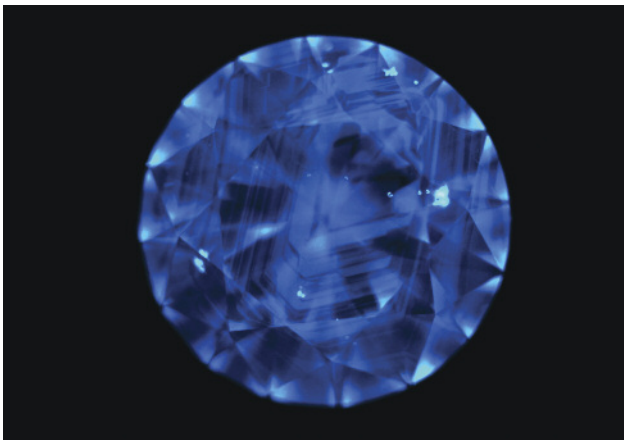

Figure 5. This DiamondView image of the host diamond shows octahedral growth zones (notice the crystal inclusions). Image by Meenakshi Chauhan.

pp. 214–226); an additional peak at about 370 nm also occurred along the o-ray. No features associated with radiation-induced color centers were present between 500 and 700 nm; these are typically observed in Maxixe-type beryls.

Standard gemological properties along with absorption spectra and the pleochroic color directions were sufficient to identify this stone as aquamarine. It displayed the most intense dichroism we have seen in an aquamarine. While there are deep sea-blue aquamarines (see O. Segura and E. Fritsch, "The Santa Maria variety of aquamarine: Never heated," *InColor*, No. 23, 2013, pp. 34–35) as well as deep blue Maxixe-type beryls, this was the deepest blue we have observed in an aquamarine with a grayish blue hue.

Gagan Choudhary (gagan@gjepcindia.com)
Gem Testing Laboratory, Jaipur, India

Color-change garnet in diamond. The Indian Gemological Institute's Gem Testing Laboratory recently examined a 0.30 ct colorless round brilliant-cut diamond containing an interesting inclusion. Infrared spectroscopy revealed features found in type IaA diamond, with a slight absorption peak due to hydrogen impurities. With a clarity grade of SI_2, the diamond contained several colorless crystals and one surface-breaking grayish green crystal (figure 4, left). Under incandescent light, the grayish green crystal appeared purplish red (figure 4, right), displaying a strong color-change phenomenon.

Under the Chelsea filter the inclusion showed a bright red reaction, suggesting the presence of chromium. There was a polished area of the included crystal on the surface, but it was too small for us to measure the refractive index.

The included crystal did not display pleochroism under microscopic observation with crossed polarizers. Viewed in immersion, it appeared to be singly refractive. DiamondView imaging showed the fluorescence pattern of growth planes found in natural diamond (figure 5). Typical octahedral growth zones of blue N3 fluorescence were evident, with no disturbance in the zones around the color-change crystal.

For conclusive identification of the inclusion, we sent the diamond to the Gem Testing Laboratory in Jaipur for laser Raman spectroscopy. As the color-change crystal

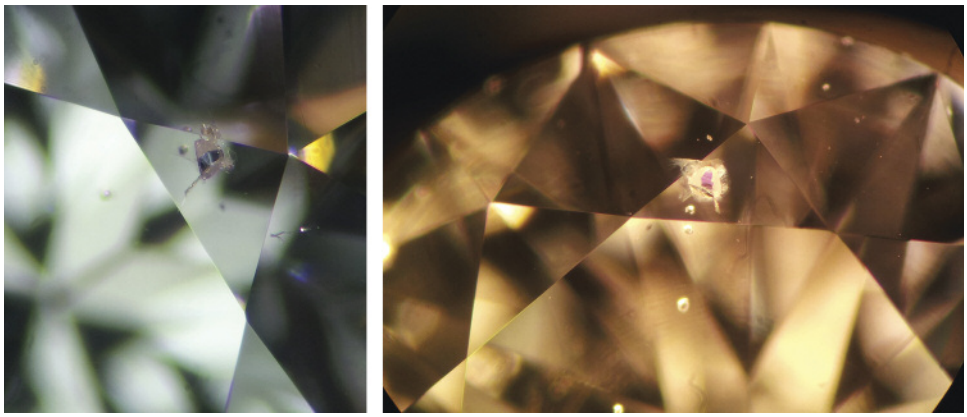

Figure 4. This inclusion, a color-change pyrope-spessartine garnet crystal in diamond, appeared grayish green in fluorescent light (left) and purplish red in incandescent light (right). Photomicrographs by Meenakshi Chauhan; field of view 2 mm (left) and 3 mm (right).

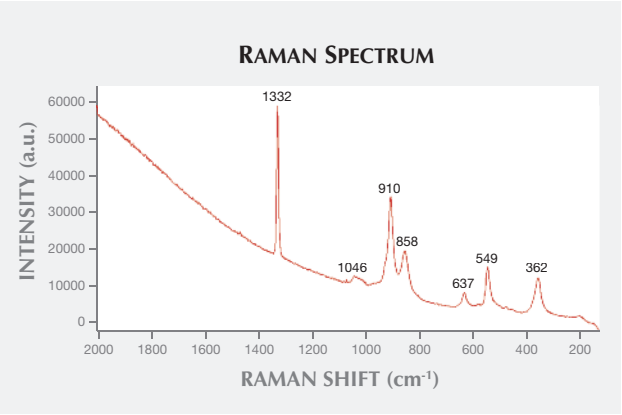

Figure 6. The Raman spectrum of the color-change pyrope-spessartine garnet inclusion showed the 1046, 910, 858, 637, 549, and 362 cm^{-1} peaks assigned to garnet. The 1332 cm^{-1} peak is assigned to diamond.

broke through the diamond's surface, a clear Raman spectrum could be obtained (figure 6). The peak at approximately 1332 cm^{-1} is assigned to diamond, and the peaks at approximately 1046, 910, 858, 637, 549, and 362 cm^{-1} are assigned to garnet. The 910 cm^{-1} peak is associated with the pyralspite isomorphous series, which is comprised of pyrope, almandine, and spessartine garnet. The inclusion was therefore identified as garnet belonging to the pyralspite series.

Meenakshi Chauhan
Indian Gemological Institute
Gem Testing Laboratory, GJEPC, New Delhi

First discovery of topazolite in Mexico. Garnet occurs in a wide variety of colors according to composition: pyrope and almandine (typically red), spessartite (brownish to orange), grossular (brown, yellow, and green), andradite (brown to black), and uvarovite (bright green). The three varieties of andradite are melanite, topazolite, and demantoid. *Topazolite*, a name that has been criticized as too similar to that of the gem species topaz, is a greenish yellow to yellow-brown andradite. According to some studies (e.g., C.M. Stockton and D.V. Manson "Gem andradite garnets," Winter 1983 *G&G*, pp. 202–208), it rarely occurs in crystals large enough to be faceted.

In January 2014, during mineralogical investigations of Mexican garnet, we made the first reported discovery of fine topazolite crystals in Mexico. These yellow to yellow-brown crystals, measuring 1.5–2.5 cm, are hosted by the Las Vigas skarn deposits (the Cerro de la Concordia mine in Las Vigas de Ramirez municipality and the Piedra Parada mine in Tatatila municipality). The deposits are located in Veracruz State, about 50 km southeast of the town of Valle de Veracruz.

The garnet composition was determined by electron microprobe, using a 41-point analysis and standard conditions of 20 kV, 20 mA, and 1 µm beam size on a JEOL JSM-35c microprobe. We chose a euhedral, relatively homogeneous crystal about 1 cm in diameter from the specimen shown in figure 7. Measurement time was 30 seconds on the peak center. The standards used were MgO for Mg, Al_2O_3 for Al, jadeite for Si, wollastonite for Ca, and elemental Fe and Mn. The electron microprobe analyses showed little compositional variation or zoning. We calculated the structural formula on the basis of 12 oxygen atoms, with the assumption of all iron as ferric. The approximate composition averaged $(Ca_{2.86}Mg_{0.06}Mn_{0.02})_{2.94}(Al_{1.20}Fe^{3+}_{0.72})_{1.92}Si_{3.03}Ti_{0.05}O_{12}$, which may be expressed as $Gr_{60.50}And_{36.70}Py_{2.80}$.

UV-visible spectroscopy showed absorption bands at 375, 416, 442, 497, and 584 nm, which can be assigned to the spin-forbidden crystal-field transition of Fe^{3+} substituted on the octahedral Al^{3+} site of the garnet structure. The correlated set of these bands also show a pattern close to that characteristic of a d^5 trivalent ion in octahedral oxygen coordination. The Mössbauer spectra were characterized by a sharp, slightly asymmetric ferrous doublet. The UV-visible and Mössbauer spectra are comparable to those reported for some garnets in previous reports (A.S. Marfunin, Ed., *Advanced Mineralogy*, Vol. 2, Springer-Verlag, Berlin, 1995, pp. 74–75, 114).

The three samples of rough topazolite (measuring 1.0–1.5 cm in longest dimension) gave the following properties: yellow-brown color; isotropic and weakly anisotropic; weak strain birefringence; RI—n_α = 1.84–1.89; hydrostatic SG—3.75–3.85; and fluorescence—inert to both long- and short-wave UV radiation.

This Mexican topazolite deposit has not been mined, and in the absence of detailed geological, mineralogical, and gemological study, no estimate of the reserves is avail-

Figure 7. This topazolite specimen is from a recent discovery in the Mexican state of Veracruz. Photo by Cristobal Castillo.

Figure 8. This giant clam pearl was recovered from a Tridacna gigas *mollusk in Papua New Guinea. Photo by Lai Tai-An Gem Lab.*

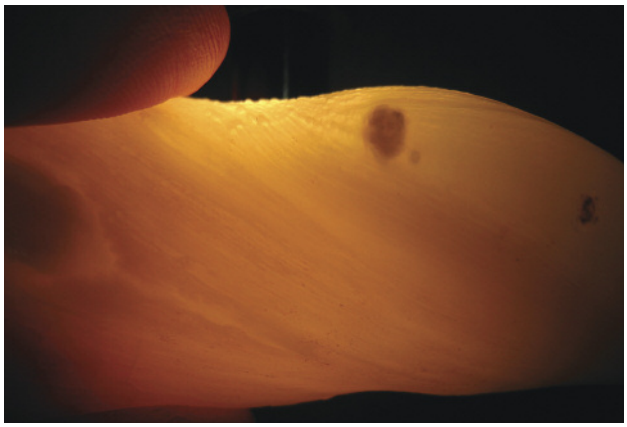

Figure 10. The Tridacna *pearl exhibited pronounced banding when viewed with transmitted light. Photo by Lai Tai-An Gem Lab.*

able. For now, there are no specimens or fashioned material from Las Vigas in the Mexican lapidary market.

Mikhail Ostrooumov (ostroum@umich.mx)
Institute of Earth Sciences (INICIT)
University of Michoacan, Morelia, Mexico

A large baroque *Tridacna gigas* (giant clam) pearl. Natural pearls from various clam species are not as rare as many believe, and plenty of samples are available in the market. But with the exception of a few very large specimens, they tend to occur in sizes under 20 carats. A client of the Lai Tai-An Gem Lab in Taipei recently requested a report on what he claimed was a natural clam pearl (figure 8) recovered from a huge *Tridacna gigas* mollusk from a fishery in Papua New Guinea in 1981.

The pearl exhibited an elongated baroque shape with uneven brown and white coloration, lacking the lustrous and shimmering iridescent colors of a nacreous pearl. It weighed 360.59 ct and measured 76.7 × 28.0 × 25.8 mm. We also recorded an SG of 2.88, which fell within the range of other *Tridacna* pearls examined in our laboratory. Long-wave UV produced a moderate chalky blue reaction. FTIR, Raman, and UV-visible spectra were collected. The Raman spectrum clearly showed that the pearl was composed of aragonite, given the peaks at approximately 142, 199, 701, and 1082 cm^{-1}. FTIR reflectance spectra also revealed calcium carbonate in the form of aragonite, with peaks at approximately 873 and 1483 cm^{-1}.

Figure 9. The natural Tridacna *pearl showed a characteristic sugary surface texture. Photo by Lai Tai-An Gem Lab; magnified 60×.*

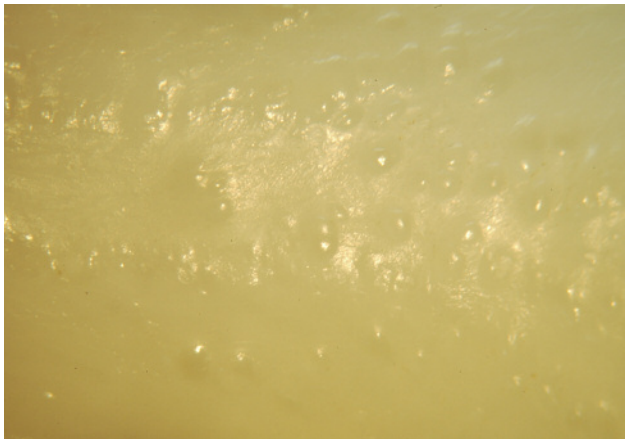

While microradiography is usually applied to the identification of pearls, it is considered especially beneficial when various types of nacreous pearls need to be separated from one another. It is usually less helpful with non-nacreous or non-porcelaneous pearls such as this one, since many reveal little in the way of helpful structure. Observed through the loupe and microscope, the pearl showed the grainy or sugary surface texture (figure 9) typical of some natural *Tridacna* pearls. This example was noteworthy for its size and interesting coloration, and its pronounced banding when viewed with transmitted light (figure 10), a feature that is often considered indicative of shell fashioned into imitation pearls. This *Tridacna* pearl was clearly no imitation.

Larry Tai-An Lai (service@laitaian.com.tw)
Lai Tai-An Gem Laboratory, Taipei

TREATMENTS

Coated fire opal in the Chinese market. Fire opal is an attractive variety of gem opal characterized by its red-orange-yellow bodycolor, with or without play-of-color. Since about 2013, the Chinese market has seen an increase in natural, synthetic (sold as Mexifire), and treated fire opals, posing identification challenges for the gemologist.

At the July 2014 Beijing Jewelry Fair, a fire opal with a rather unusual orange bodycolor (figure 11) attracted our

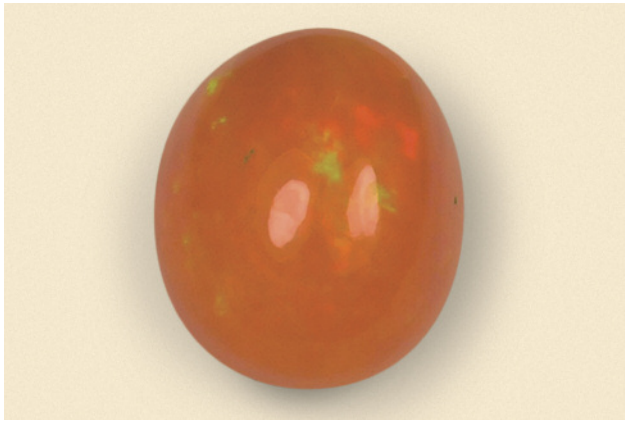

Figure 11. This 3.87 ct translucent orange fire opal with play-of-color was identified as a coated stone. Photo by Wen Han.

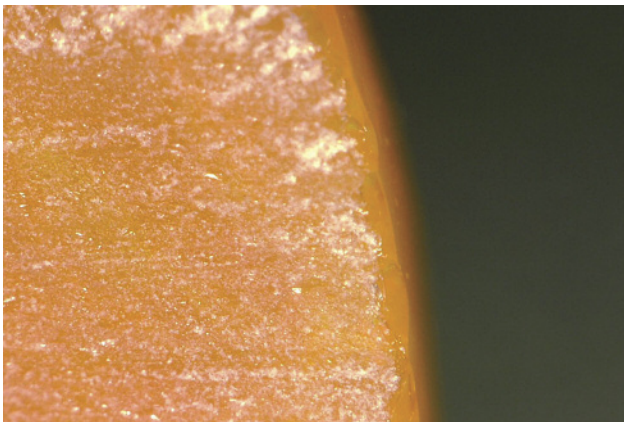

Figure 13. A cross-section image of the fire opal shows a coated surface layer about 60–90 µm thick. Photo by Wen Han; magnified 100×.

interest. It was a 3.87 ct oval cabochon with fair play-of-color, measuring approximately 14 × 10 × 6 mm. Its spot RI of about 1.39 and hydrostatic SG of 1.85 were both lower than the values for most natural fire opal. It was inert to both long- and short-wave UV radiation; untreated fire opal may also be inert to UV radiation or show green and blue fluorescence. Magnification revealed obvious scratching and small pits on the surface (figure 12), suggesting a lower hardness and the presence of a coating. We cut the sample in half for further examination. High magnification clearly showed the boundary between the orange layer and the substrate, which was also orange opal. The coated layer was about 60–90 µm thick (figure 13).

EDXRF chemical analysis detected mainly Si and minor amounts of Ca, Na, and K. Fourier-transform infrared (FTIR) and Raman spectroscopy were used to identify the coating. Infrared reflectance spectroscopy revealed three strong bands at 1099, 789, and 474 cm^{-1} that are related to the fundamental Si-O vibrations, as expected for natural fire opal. Then we scraped off the coating with a razor blade to obtain its infrared transmittance spectrum. The peaks, specifically those at 2926, 1729, 1451, and 1159 cm^{-1}, indicated the presence of organic matter consistent with acrylic polymer (figure 14). The Raman scattering spectra of the fire opal revealed several peaks attributed to both the substrate opal and the coating (figure 15). The Raman bands at about 350, 785, and 1080 cm^{-1}, due to different stretching and bending vibration modes of the Si-O system, are typical for opal-CT. Other peaks, including 1320 and 1610 cm^{-1}, are attributed to the acrylic coating material. Acrylic coatings are applied to various gem materials, such as lapis lazuli and jadeite (Summer 1992 Gem News, p. 135). This coating of acrylic polymer was used to enhance the fire opal's color and seal its fissures. The coating also lowered the stone's RI and SG values.

Our investigation, believed to be the first report of coated fire opal in the Chinese market, reinforces the need

Figure 12. Surface scratches and small pits were visible on the coated fire opal. Photo by Wen Han.

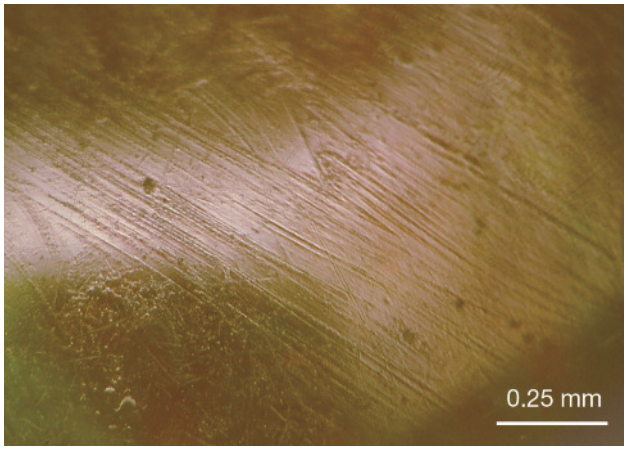

Figure 14. The FTIR spectrum of the coating scraped from the surface of the fire opal exhibits characteristic peaks at 2926, 1729, 1451, and 1159 cm^{-1} consistent with acrylic polymer.

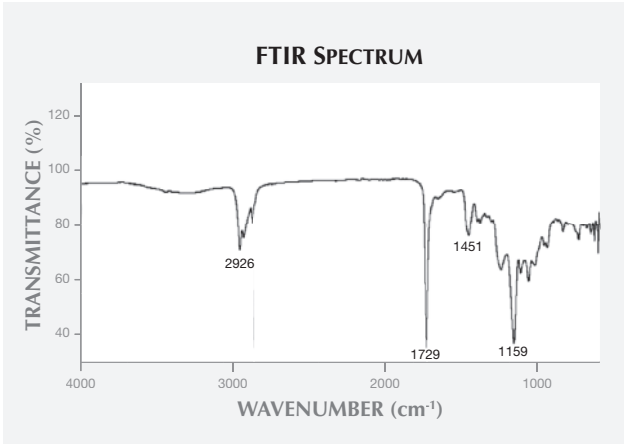

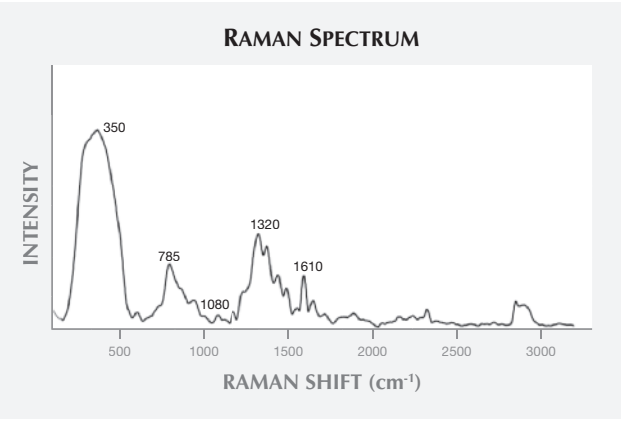

Figure 15. Raman bands at approximately 350, 785, and 1080 cm^{-1} are typical for opal-CT; the other peaks, including those at 1320 and 1610 cm^{-1}, are attributed to the acrylic coating.

for caution when buying these products. This coated fire opal's lower RI and SG values, combined with magnification and Raman spectroscopy, are effective and nondestructive means of identification.

Wen Han (winnerzx@126.com), Taijin Lu, Hua Chen, and Jian Zhang
National Gems & Jewelry Technology Administrative Center (NGTC) BeijingT

CONFERENCE REPORTS

IMA General Meeting. The 21st General Meeting of the International Mineralogical Association (IMA) was held September 1–5 in Johannesburg, South Africa. Several oral and poster presentations were presented in a session on gem materials.

Giovanna Agnosi (University of Bari, Italy) discussed preliminary results of an X-ray diffraction topography study of Colombian trapiche emeralds, which revealed a consistent crystallinity between the arms and the hexagonal core. She presented a model of trapiche formation in which the growth of the hexagonal core occurred first, followed by the six arm sections. **Ulrika D'Haenens-Johansson** (GIA, New York) outlined the status of synthetic diamond production. She reviewed the means of identification based on visual observations, structure-related ultraviolet fluorescence reactions, and distinctive spectroscopic features. In concluding, she noted that synthetic diamonds can be unequivocally recognized by major gem laboratories.

Andrew Fagan (University of British Columbia, Vancouver) presented the geologic setting and a model of formation of the Fiskenæsset corundum district in southwest Greenland. Estimates of ore reserves suggest that this could become a commercial ruby deposit. **Gaston Giuliani** (Centre de Recherches Pétrographiques et Géochimiques, Nancy, France) studied the oxygen isotope and trace-element chemistry of sapphire xenocrysts in basalts from Changle, China, and of corundum from the Mbuyi-Mayi kimberlite in the Democratic Republic of Congo, to trace their primary sources. In both cases, the host basalt and kimberlite transported the corundum crystals from the lower crust and upper mantle.

Daniel Ichang'i (University of Nairobi) described efforts by the Kenyan government to document and better understand the geologic setting of the country's numerous gem deposits. He discussed two main occurrence lithologies: the metamorphic rocks of the Neoproterozoic Mozambique orogenic belt, and the Paleogene-Neogene basaltic volcanics in the Northern and Central Kenya rift regions.

Stefanos Karampelas (Gübelin Gem Lab, Lucerne, Switzerland) detailed the gemological characteristics of emeralds from Itatitia in Minas Gerais, Brazil. The emeralds formed along the contact between phlogopite schists and highly evolved granitic pegmatites. Based on minor and trace-element chemistry, they can be distinguished from emeralds from other Brazilian and world deposits. **Vincent Pardieu** (GIA, Bangkok) gave a talk about Montepuez in northern Mozambique, which is currently the world's largest source of rubies. He also presented a short film about GIA expeditions he has led to gem deposits in eastern Africa. **Wuyi Wang** (GIA, New York) presented a study of carbon isotopes of synthetic and natural diamonds. The latter displayed $\delta^{13}C$ values from 0 to –20‰, while the former ranged from –25 to –75‰.

Christopher M. Breeding (GIA, Carlsbad, California) described the interesting features of alluvial diamonds from the Marange deposit in eastern Zimbabwe. These type Ia diamonds display surface radiation staining, aggregated nitrogen impurities, and elevated hydrogen impurity contents, but these features do not provide a reliable indicator of geographic origin. **Julien Feneyrol** (Centre de Recherches Pétrographiques et Géochimiques, Nancy, France) presented a model of the metamorphic formation of tsavorite nodules in primary deposits. The tsavorite nodules are always contained within graphitic gneiss and calc-silicates with intercalations of marble. **Elena Sorokina** (Fersman Mineralogical Museum, Moscow) described a model of ruby and sapphire formation in marbles at Snezhnoe in Tajikistan.

James E. Shigley
GIA, Carlsbad, California

ERRATA

1. The S. Saeseaw et al. emerald inclusions article in the Summer 2014 issue (pp. 114–132) listed the photomicrograph image widths ten times larger than their actual width.

2. The Summer 2014 Gem News International section (pp. 158–159) erroneously cited "absorption peaks" in the Raman spectrum of a jadeite bangle. We thank Thierry Cathelineau for bringing this to our attention.